Hydrogen-affected fatigue crack propagation at various loading frequencies and gaseous hydrogen pressures in commercially pure iron

Tomoki Shinko, Gilbert Hénaff, Damien Halm, Guillaume Benoit, Giovambattista Bilotta, Mandana Arzaghi

Version of Record: https://www.sciencedirect.com/science/article/pii/S0142112318305668
Manuscript_df731409dbc3c3fbefd8989854f56d26

Hydrogen-affected fatigue crack propagation at various loading frequencies and gaseous hydrogen pressures in commercially pure iron

Tomoki SHINKO[1], Gilbert HENAFF[1], Damien HALM[1], Guillaume BENOIT[1], Giovambattista BILOTTA[1] and Mandana ARZAGHI[1]

[1]Institut Pprime, UPR 3346 CNRS- ISAE-ENSMA- Université de Poitiers, France

Keywords: Hydrogen embrittlement, Fatigue crack propagation, Commercially pure iron, Intergranular fracture, Crack tip plasticity

Abstract

Hydrogen-Affected Fatigue Crack Growth (HAFCG) in commercially pure iron has been characterized in terms of hydrogen gas pressure, loading frequency and stress intensity factor range ΔK. A higher hydrogen gas pressure decreases the critical value of ΔK triggering the HAFCG enhancement, and a lower loading frequency increases the HAFCG enhancement. Intergranular FCG in the non-accelerated regime is likely caused by the hydrogen-induced microvoid coalescence along the grain boundary, while a brittle cyclic cleavage fracture in the accelerated regime can be explained in terms of a synergy of crack tip sharpening and hydrogen-enhanced decohesion process.

1. Introduction

In coming years, due to a shortage of fossil fuels and air pollution problem, the development of "fossil-fuel-free" society will be strongly required for sustainable development of society. One of the most promising solutions to achieve this goal is a clean hydrogen-based society whose sustainable infrastructure does not consume fossil fuels and does not emit greenhouse gases. For example, a fuel cell vehicle and a hydrogen refueling station already have been developed in the industry [1]. However, a key issue related to the development of such infrastructures is hydrogen compatibility of the materials used. Indeed it is well known that metallic materials exposed to gaseous hydrogen may undergo a significant degradation of mechanical properties recognized as "hydrogen embrittlement" [2–4]. In particular, a fatigue crack growth resistance reduces remarkably [3,5], which is recognized as a serious problem in guaranteeing the long-term reliability of the hydrogen-related equipment. Hence the elucidation of its mechanism is highly demanded.

Since the hydrogen embrittlement of iron and steels was firstly found by Johnson [6] in 1874, many types of research have been conducted for investigating an effect of hydrogen on the mechanical properties of metallic materials. At the same time, numerous theories have been proposed to explain the mechanism of hydrogen embrittlement. In particular, the following three theories are considered as the most important ones: HEDE (Hydrogen-Enhanced DEcohesion) [7,8], HELP (Hydrogen-Enhanced Localized Plasticity) [9], and AIDE (Adsorption-Induced Dislocation Emission) [10]. The HEDE mechanism supposes that the hydrogen atoms adsorbed at a crack tip or segregated at the grain boundaries weaken interatomic bonds and cause an atomic decohesion. This leads to a brittle fracture such as a cleavage-like fracture and an intergranular decohesion. In the HELP mechanism, the solute hydrogen atoms in front of the crack tip enhance and localize the dislocation activity. This may promote a nucleation and coalescence of microvoids as crack embryos, resulting in a crack propagation with less blunting and less macroscopic ductility of the material. The fracture surface often exhibits small, shallow dimples [11,12]. The AIDE mechanism is based on the facilitation of dislocation emission due to adsorbed hydrogen atoms. In this mechanism, the adsorbed hydrogen on the surface or the sub-surface weakens

interatomic bonds and promotes the dislocation nucleation at the crack tip which enhances the local plastic strain near the crack tip. The principle of Fatigue Crack Growth (FCG) enhancement by AIDE is similar to the HELP mechanism. However, the main difference is that AIDE involves the adsorbed hydrogen in sub-surface while the effect of HELP is caused by the solute hydrogen in the material.

Over the last decades, most of the studies concerning hydrogen embrittlement have focused on a framework of fracture under monotonic loading. In addition to this, research on materials in the hydrogen-charged state has been common due to its easiness. However, from the viewpoint of practical application of hydrogen-related equipment, the material is subjected to a hydrogen gas environment and repeated loading. Since hydrogen distribution in the material exposed to the hydrogen atmosphere is different from the charged case, this configuration has to be specifically addressed [11]. Therefore, it is practically important to consider a problem of fatigue in a state of exposure to a hydrogen gas environment.

From this fact, in recent years, the influence of hydrogen on fatigue life has been actively investigated. A significant enhancement of Fatigue Crack Growth Rate (FCGR) under the hydrogen-charged state and gaseous hydrogen atmosphere have been revealed [3,5]. Especially, martensitic [13] and ferrite-pearlite steels [3] exhibit a high susceptibility to hydrogen effect mainly contributed by their high diffusivity of hydrogen.

Matsuoka et al. [14,15] noticed that the localization of plastic deformation near the crack tip is associated with the FCGR enhancement in hydrogen-charged austenitic stainless steel and low carbon steel, by observing the suppression of slip deformation near the crack path and the presence of brittle-like striation on the fracture surface. They proposed a model of hydrogen-assisted FCG called as “Hydrogen Enhanced Successive Fatigue Crack Growth (HESFCG)” model. On the other hand, Nishikawa et al. [16] proposed a FCG model associated with hydrogen-induced nucleation and coalescence of microvoid ahead of the crack tip, namely a ductile fracture process at micro-scale. From these recent studies, the modification of plasticity at the crack tip by hydrogen has been recognized as a key factor of HAFCG mechanism. The hydrogen effect on crack tip plasticity has been evidenced by various means of observation techniques such as Electron Back Scattering Diffraction (EBSD) [17,18] and Transmission Electron Microscopy (TEM) [17–20]. Especially, Robertson et al. [12,21,22] have been leading an advancement of fundamental understanding of the interaction between solute hydrogen and mobile dislocations in the material by means of an in-situ TEM technique.

It also has been reported that the HAFCG rate depends on hydrogen gas pressure and loading frequency: a higher hydrogen gas pressure or a lower loading frequency lead to a higher FCG enhancement [13,23]. The recent finding made by several researches [14,24–27] is the presence of an upper limit of HAFCG rate increase by decreasing loading frequency down to f = 0.01 Hz in hydrogen-charged low-carbon steel. Subsequently, Yoshikawa et al. [27,28] found out in low carbon steel under hydrogen gas environment that, when one keeps decreasing the loading frequency lower than the values at which HAFCG rate reaches the upper limit, the FCGR significantly decreases. This result was contrary to the conventional understanding that the HAFCG rate increases as the loading frequency decreases. Yoshikawa et al. proposed that the gradient (and not only the value) of hydrogen concentration ahead of the crack tip can be involved in a criterion to determine the onset of hydrogen effect on FCGR. Even though the dependence of HAFCG rate on hydrogen gas pressure and loading frequency has been examined as mentioned above, however how hydrogen gas pressure and loading frequency influence the HAFCG mechanism is not clarified yet.

Meanwhile, the numerical tool predicting the HAFCG based on a cohesive zone model has been developed [29,30]. It has been found to correctly predict HAFCG rate at low hydrogen gas pressure (0.09

MPa), while it underestimated highly enhanced FCGRs at high hydrogen gas pressure (9 MPa) in precipitation-hardened martensitic stainless steel 15-5PH. This result indicates that further understanding of the influence of hydrogen gas pressure and loading frequency on the HAFCG mechanism is required to improve the capability of the numerical model.

In this point of view, the recent studies by Pprime institute [23,31,32] have put the emphasis on FCG tests in a commercially pure iron, Armco iron, aiming to investigate the fracture mechanism under various hydrogen gas pressures and loading frequencies. Armco iron was selected as a sample material because it allows us to analyze the interaction between hydrogen and its simple ferrite microstructure. From the previous studies, it has been shown that the FCGR at hydrogen gas pressure P_{H2} = 35 MPa is highly enhanced in this material [23]. Besides, the clear dependence of HAFCG rate on the loading frequency has been observed in the range of f = 0.2 - 20 Hz. It is nevertheless necessary to investigate further the influence of hydrogen gas pressure, as well as a loading frequency on the FCGRs and the fracture mechanism.

The objective of this study is to understand a dependency of HAFCG on a hydrogen gas pressure and a loading frequency and its mechanism. For this objective, additional fatigue crack propagation tests in Armco iron under a fixed hydrogen gas pressure P_{H2} = 3.5 MPa have been conducted at two loading frequencies, f = 2 and 20 Hz. A fracture mode, a crack tip plasticity, and a hydrogen distribution ahead of the crack tip were analyzed for the tested specimens for understanding a mechanism of hydrogen effect on FCGR. Finally, on the basis of an obtained experimental insight as well as previously obtained results of STEM observations [32], a mechanism of HAFCG and its dependency on a hydrogen gas pressure, a loading frequency, and a stress intensity factor range ΔK were discussed.

2. Material and testing method

The material used in this study is a commercially pure iron, Armco iron (AK Steel Corp.). The chemical composition of Armco iron is shown in Table 1. An annealing heat treatment at 1073K (800 °C) for 60 minutes was applied in order to relax residual stresses and homogenize the ferrite microstructure. Fig. 1 shows the EBSD mapping of the heat-treated Armco iron. The average grain size after the heat treatment is approximately 90 μm. The mechanical properties determined after heat treatment are yield strength σ_y = 170 MPa, maximum elongation A = 25 %, and tensile strength σ_{TS} = 280 MPa.

Table 1 Chemical composition of Armco iron (mass %).

Element	C	Mn	P	S	Cu	N	Al
Content	0.001	0.050	0.003	0.003	0.009	0.004	0.005
Element	Cr	Mo	Ni	Sn	Si	Fe	
Content	0.015	0.002	0.14	0.002	0.004	Balance	

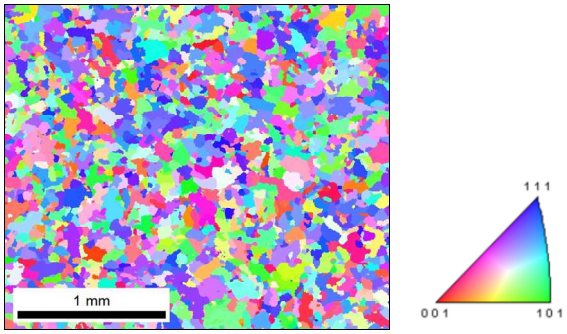

Fig. 1 EBSD mapping of the microstructure of Armco iron used in this study. The average grain size is about 90 µm.

Specimen preparation and fatigue crack propagation tests were performed by following the ASTM E647 standard. CT specimens with a width W = 40 mm and a thickness B = 8 mm were machined in the longitudinal-transversal plane against hot-rolling direction. The specimen surface was finished by diamond abrasives with 1 µm diameter. Fatigue crack propagation tests were conducted by a loading control at room temperature under gaseous hydrogen at hydrogen gas pressure P_{H2} = 3.5 MPa. The amount of impurities (water vapor and oxygen) of hydrogen gas was 18 and 10 ppm, respectively. The tests were performed by using Hycomat test bench [13] developed by Pprime institute. This test bench consists of an autoclave assembled to a servo-hydraulic load-frame, which has a capacity to perform mechanical tests under the maximum gas pressure of 40 MPa at the highest temperature of 150 °C (423 K). The various loading frequencies of 2 and 20 Hz were applied to investigate its influence on the FCGR. Crack length was measured by optical microscopy and Direct Current Potential Drop (DCPD) technique during the tests. The stress ratio (K_{min}/K_{max}) was 0.1, where K_{min} and K_{max} are the minimum and maximum stress intensity factors, respectively.

3. Result

3.1. Fatigue crack propagation rate

The results of FCGR (da/dN, where a the crack length and N the number of cycles) at hydrogen gas pressure P_{H2} = 3.5 MPa are presented in Fig. 2 as well as the results at P_{H2} = 35 MPa previously obtained [23,31]. In Fig. 2, one can see that the FCGRs at both hydrogen gas pressures are higher than the ones in the inert environments: air, nitrogen, and vacuum. In addition, the FCGRs in hydrogen exhibit different trends depending on ΔK value. Three distinct regimes can be defined, typically by considering for example the curve at P_{H2} = 35 MPa and f = 0.2 Hz:

a) A non-accelerated regime (ΔK < 12 MPa×m$^{1/2}$): in the low ΔK range, the FCGR in hydrogen is similar to the FCGR in the air.
b) A transition regime (12 < ΔK < 14 MPa×m$^{1/2}$): the FCGR in hydrogen sharply increases up to 50 times higher than that in the air.
c) An accelerated regime (14 MPa×m$^{1/2}$ < ΔK): after the transition regime, the slope of the curve in hydrogen is nearly similar to the one in the air but the FCGRs are significantly enhanced.

This type of FCGR trend with the presence of a characteristic “knee” also has been determined in pipeline steels [5,24,33–36]. This fact that Armco iron, i.e. a pure ferrite microstructure, exhibits the similar sensitivity to hydrogen as pipeline steels, suggests that the overall behavior is mainly contributed

by the interaction between hydrogen and ferrite microstructure and that pearlite microstructure only plays a minor role.

In terms of the influence of loading frequency, the higher magnitude of the acceleration of FCGR is exhibited at a lower frequency. The difference of the FCGRs at 35 MPa hydrogen between 0.2 Hz and 2 Hz is smaller compared with that between 2 and 20 Hz.

In terms of the influence of hydrogen gas pressure, when comparing the FCGR curves at f = 2 Hz and P_{H2} = 3.5 and 35 MPa, the ΔK value at the beginning of the transition regime, ΔK_{tr}, at P_{H2} = 35 MPa is lower ($\Delta K_{tr} \approx 11$ MPa×m$^{1/2}$) than that at P_{H2} = 3.5 MPa ($\Delta K_{tr} \approx 15$ MPa×m$^{1/2}$). The dependency of ΔK_{tr} on the hydrogen gas pressure has also been confirmed in a precipitation-hardened martensitic stainless steel [37] and in a low carbon steel [28,38]. The FCGR curves at P_{H2} = 3.5 MPa ended in the transition regime, and the accelerated regime was not confirmed within the investigated range of ΔK.

The HAFCG rate in a commercially pure iron has also been investigated by Ogawa et al. [18,39,40]. They used a JIS-C2504 grade as a material. The comparison between the FCGRs in the present study and the ones in hydrogen (at P_{H2} = 0.2, 0.7, 20, 90 MPa and f = 1, 5 Hz) and in the air (f = 1 Hz) from their studies is presented in Fig. 3. Some of the FCGR curves of JIS-C2504 in hydrogen exhibit similar characteristic regimes (non-accelerated, transition and accelerated) to the ones observed in this study. The FCGR curves of JIS-C2504 clearly show the dependency on hydrogen gas pressure, i.e. the shift of ΔK_{tr}, similar to this study. Note also that there is no influence of hydrogen gas pressure on the magnitude of FCGR acceleration in the accelerated regime.

These dependences of HAFCG rate on hydrogen gas pressure and loading frequency are schematically summarized in Fig. 4. As illustrated in Fig. 4, a lower loading frequency results in a higher magnitude of HAFCG enhancement in the accelerated regime, meanwhile, a higher hydrogen gas pressure results in a lower ΔK value triggering HAFCG acceleration (ΔK_{tr}).

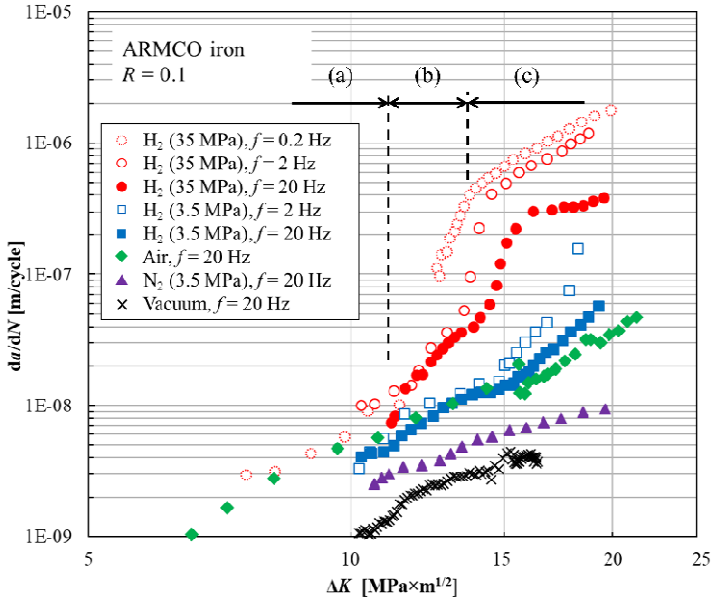

Fig. 2 FCGRs (= d*a*/d*N*) vs Δ*K* in Armco iron at various hydrogen gas pressures and loading frequencies [23,31].

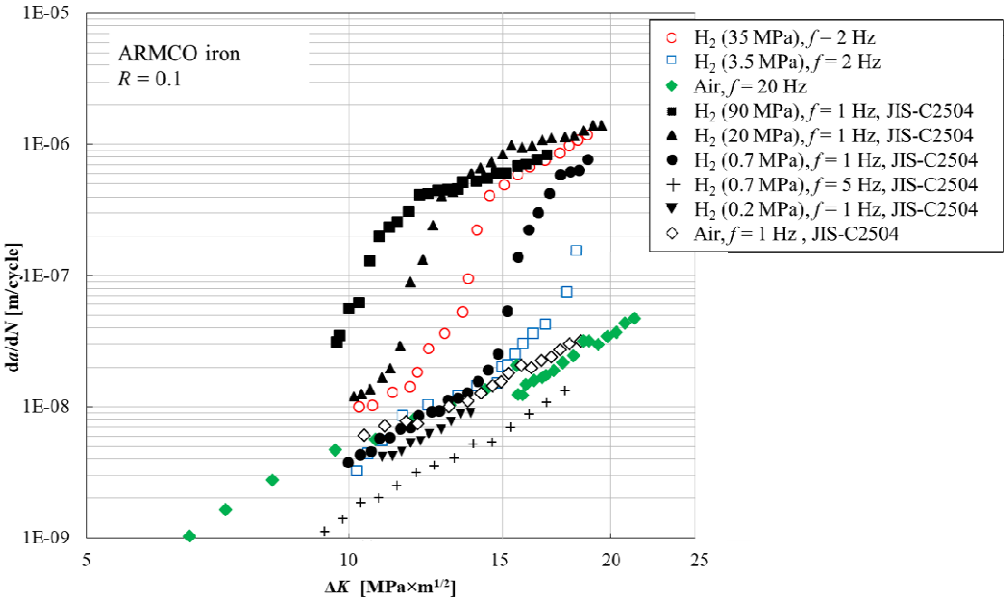

Fig. 3 Comparison between the FCGRs in Armco iron and the ones in commercially pure iron, JIS-C2504, in hydrogen and in air obtained by Ogawa et al. [18,39,40].

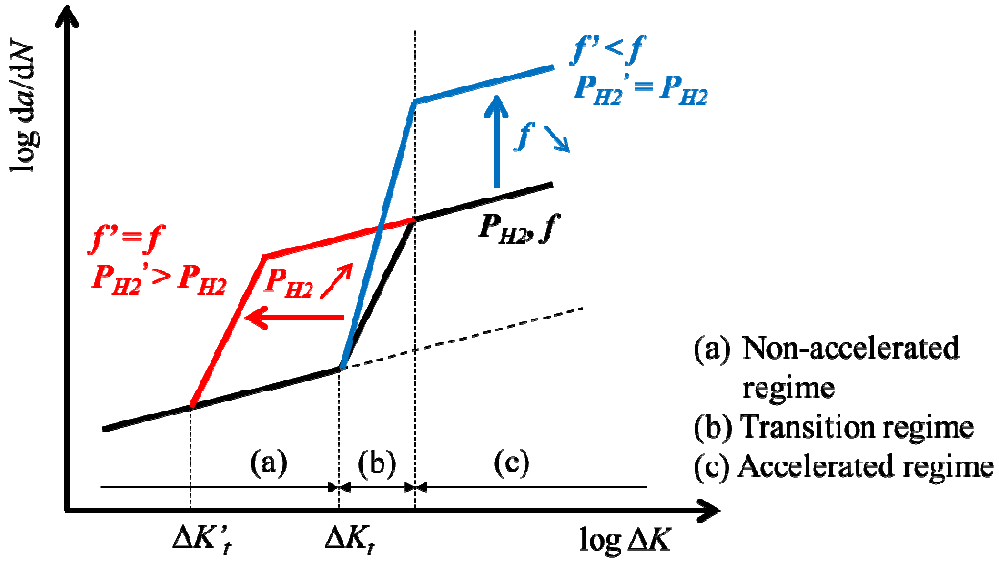

Fig. 4 Schematic diagram of the influence of hydrogen gas pressure and loading frequency on FCGR curve.

3.2. Fracture surface observation

In the previous section, the drastic acceleration of FCGR due to hydrogen has been observed from the intermediate to the higher value of ΔK. To investigate the fracture mechanism of HAFCG, the fracture surface was observed by means of SEM. The SEM images of the fracture surface in air and gaseous hydrogen at P_{H2} = 35 and 3.5 MPa are shown in Fig. 5, Fig. 6 and Fig. 7, respectively. The fracture surfaces at ΔK = 8 and 15 MPa×m$^{1/2}$ in the air (Fig. 5a and b, respectively) represent a typical ductile transgranular fracture. This fracture mode continued until the unstable rupture at the end of the test.

On the other hand, the fracture surface in hydrogen at P_{H2} = 35 MPa, f = 20 Hz, ΔK = 8 MPa×m$^{1/2}$ (Fig. 6a, in the non-accelerated regime) was fully covered by intergranular facets evidencing an intergranular fracture. The observation of the intergranular facets at higher magnification (the area indicated by the red box in Fig. 6a) is shown in Fig. 6b: the presence of regularly spaced stripe-like markings is noticed on the surface of the intergranular facets. The orientation of these markings is globally perpendicular to the macroscopic crack propagation direction (from left to right in the images). The same type of intergranular fracture was observed at the other loading frequencies (f = 0.2 and 20 Hz) and at the hydrogen gas pressure P_{H2} = 3.5 MPa while not shown here. Fig. 6c-e and Fig. 7 show the fracture surfaces at ΔK = 18 MPa×m$^{1/2}$ (in the accelerated regime) at P_{H2} = 35 and 3.5 MPa, respectively. In the transition regime, the intergranular facets in hydrogen have been gradually replaced by transgranular fracture surface with the increase of ΔK. Subsequently, in the accelerated regime, the fracture surface became fully transgranular fracture surface with many tear ridges and some flat surface parts at all the loading frequencies as shown in Fig. 6c-e and Fig. 7. In addition, coarse striations with small undulation, i.e. brittle-like striations, were observed on the flat surface parts as shown in the image at higher magnification (Fig. 6f). No clear difference in the fracture surfaces at different hydrogen gas pressures and different loading frequencies was confirmed. Birenis et al. [40,41] have observed that the transgranular crack propagation in hydrogen exhibiting the flat fracture surface is along a {100}-type cleavage plane in the grains by means of EBSD analysis in pure iron. They concluded that the fracture mode in the accelerated regime is Quasi-Cleavage (QC) fracture with a formation of brittle-like striations.

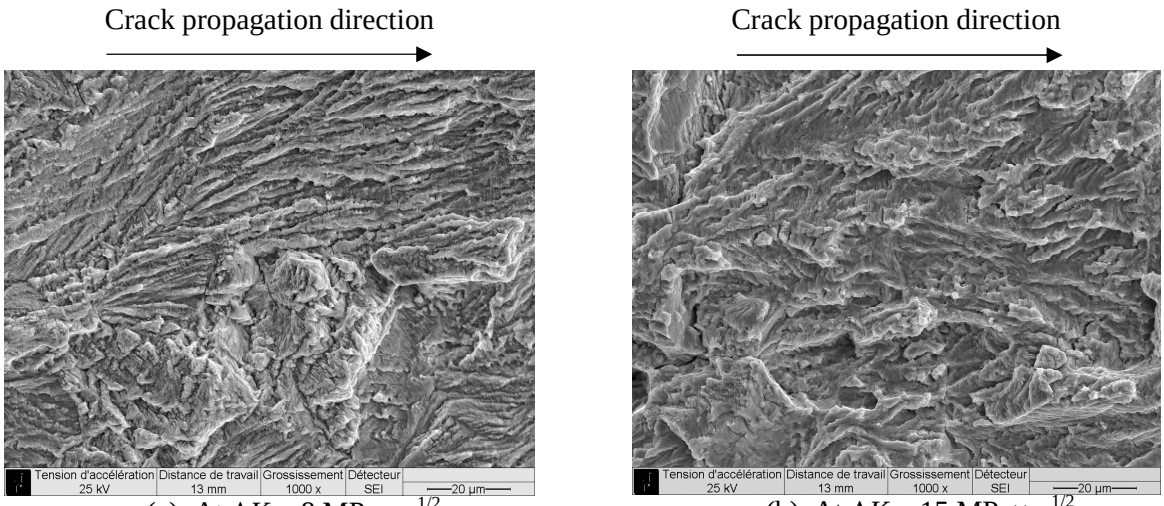

(a) At ΔK = 8 MPa×m$^{1/2}$ (b) At ΔK = 15 MPa×m$^{1/2}$

Fig. 5 SEM images of fracture surfaces under air (at f = 20 Hz) at ΔK = 8 and 15 MPa×m$^{1/2}$ shown in (a) and (b), respectively.

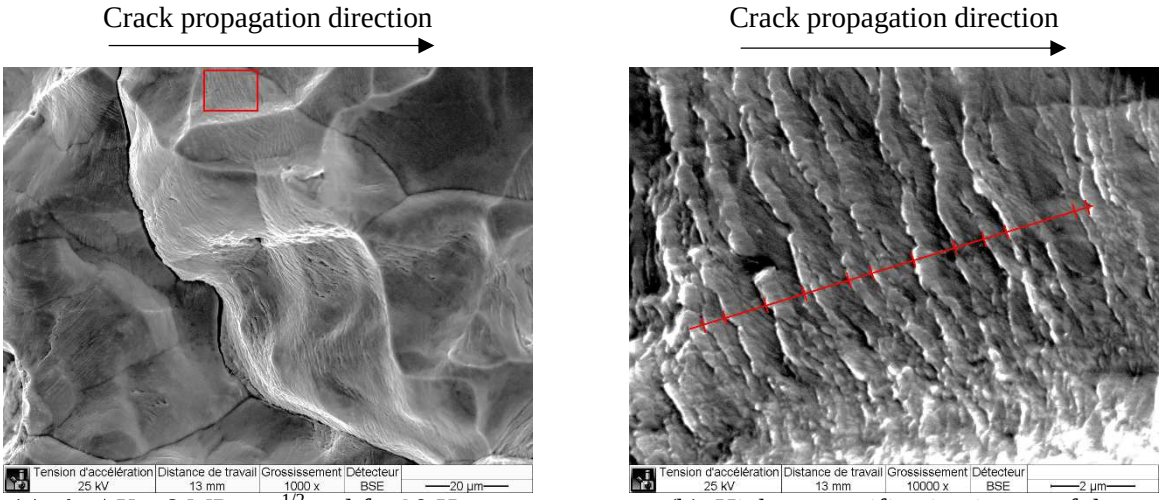

(a) At ΔK = 8 MPa×m$^{1/2}$ and f = 20 Hz.

(b) Higher magnification image of the intergranular facet indicated by the red box in the image (a). The red line in this figure shows an example of a gauge line (10 µm) to measure a spacing of the plastic markings.

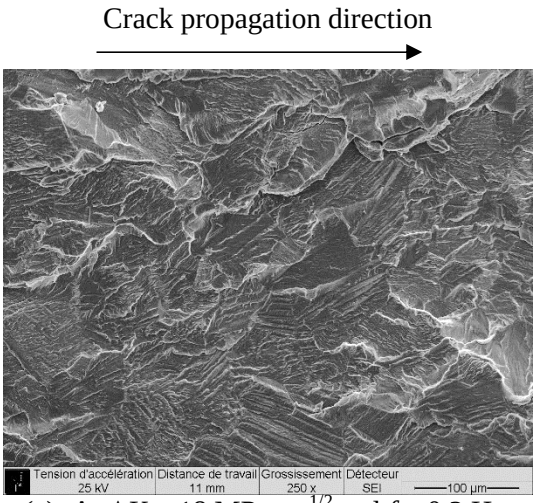

(c) At ΔK = 18 MPa×m$^{1/2}$ and f = 0.2 Hz.

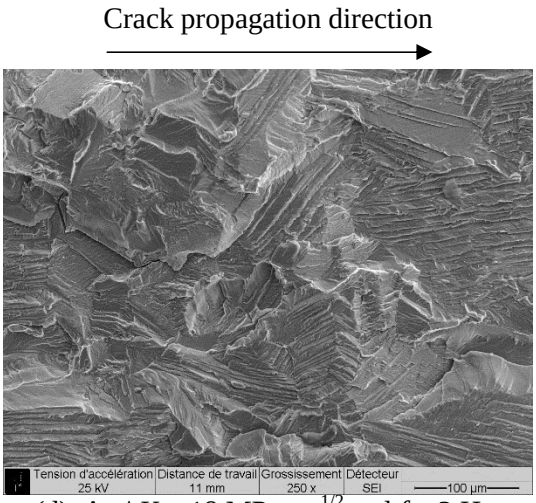

(d) At ΔK = 18 MPa×m$^{1/2}$ and f = 2 Hz.

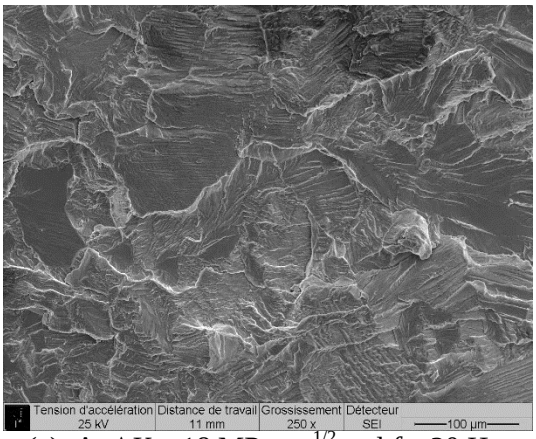

(e) At ΔK = 18 MPa×m$^{1/2}$ and f = 20 Hz.

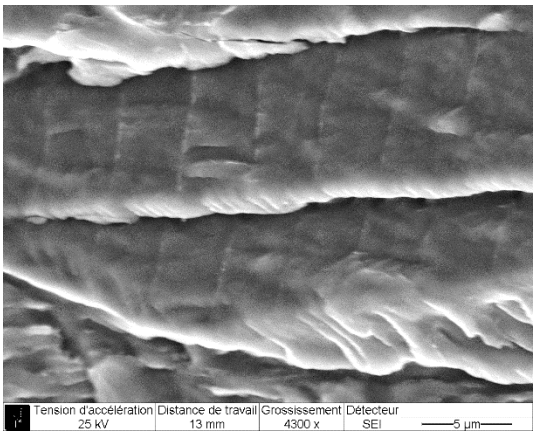

(f) Higher magnification image of brittle-like striation at ΔK = 20 MPa×m$^{1/2}$ and f = 2 Hz.

Fig. 6 SEM images of fracture surfaces under gaseous hydrogen at P_{H2} = 35 MPa, f = 0.2, 2 and 20 Hz. A crack growth direction is from left to right in these images.

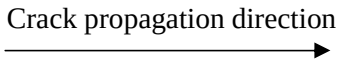

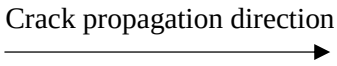

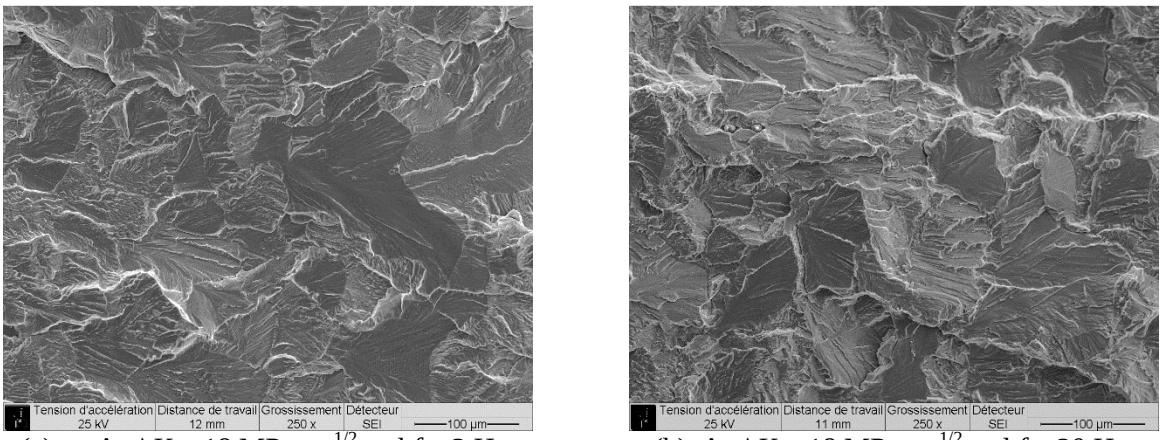

(a) At ΔK = 18 MPa×m$^{1/2}$ and f = 2 Hz. (b) At ΔK = 18 MPa×m$^{1/2}$ and f = 20 Hz.

Fig. 7 SEM images of fracture surfaces under gaseous hydrogen at P_{H2} = 3.5 MPa, f = 2 and 20 Hz. A crack growth direction is from left to right in these images.

3.3. Surface topography of side surface near the crack path

In order to investigate the influence of hydrogen on the plastic deformation in vicinity of the crack tip, surface topography (height variation) of the side surface near the fatigue crack path has been measured on the tested CT specimens by means of an interferometric confocal microscopy (Talysurf CCI6000, Taylor Hobson). The in-plane and out-of-plane resolutions of the measurement were 0.35 µm and 0.05 nm, respectively (according to the manufacturer). The obtained surface topographic images of the specimens at ΔK = 18 MPa×m$^{1/2}$ in nitrogen and hydrogen are shown in Fig. 8. In these images, the surface height variation is indicated by the color gradation from blue to red. The green color part corresponds to the original surface height without any displacement. The blue vertical part in the middle of the images is the crack path. In Fig. 8a showing the surface topography near the crack path in nitrogen, an uneven surface was observed over a range of few hundreds of µm from the crack path. According to Rice [42], the cyclic plastic zone size (diameter) Δr_p in a plane stress condition can be estimated by the following equation:

$$\Delta r_p = \frac{1}{\pi}\left(\frac{\Delta K}{2\sigma_y}\right)^2 \quad (1)$$

The value of half cyclic plastic zone size $\Delta r_p/2$ at ΔK = 18 MPa×m$^{1/2}$ is calculated as 446 µm. Since the surface unevenness in nitrogen (Fig. 8a) spreads out within a 200 - 300 µm distance from the crack path which is in the same order of magnitude to the calculated value of $\Delta r_p/2$, thus this surface unevenness is likely produced by cyclic plastic deformation in the vicinity of the crack tip.

On the other hand, Fig. 8b-f show the surface topographies near the crack path in hydrogen at the same value of ΔK, hydrogen gas pressures P_{H2} = 3.5 and 35 MPa, and loading frequencies f = 0.2, 2 and 20 Hz. At f = 0.2 Hz and P_{H2} = 35 MPa (in Fig. 8b, only a half of the specimen was available for measurement). All the surface topographic images in hydrogen show homogeneous green color, meaning no evident surface unevenness. This result indicates that a reduction of cyclic plastic deformation near the crack tip occurred in the accelerated regime.

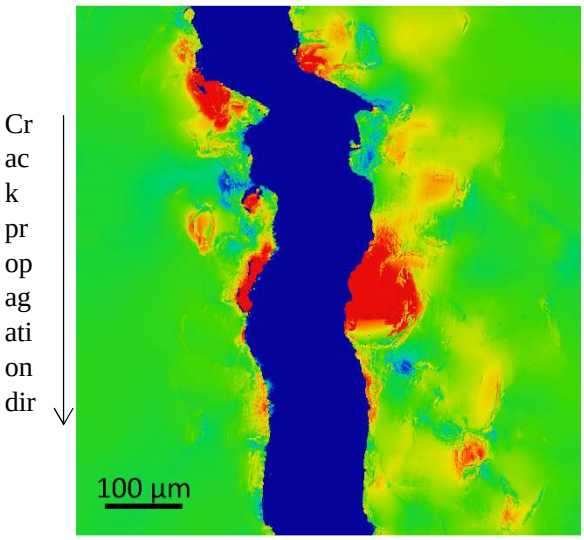

(a) At f = 20 Hz in nitrogen of 3.5 MPa.

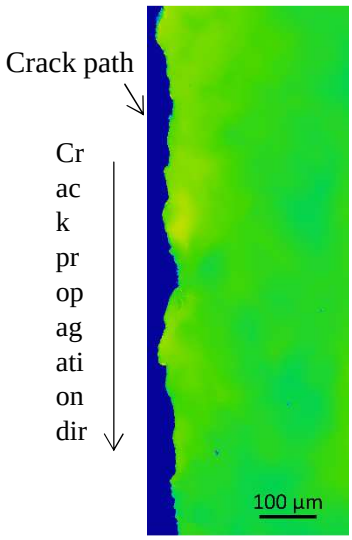

(b) At f = 0.2 Hz in hydrogen of P_{H2} = 35 MPa.

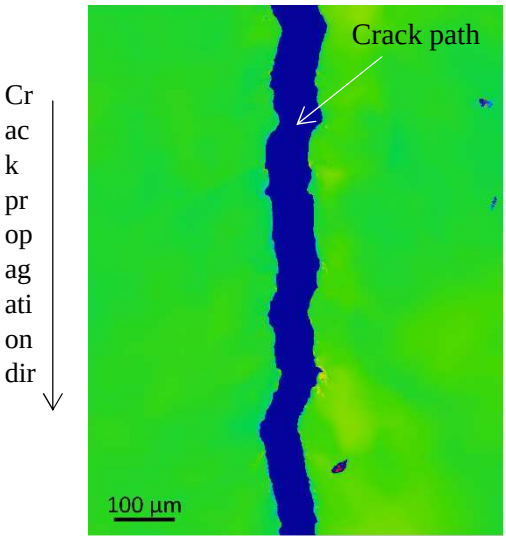

(c) At f = 2 Hz in hydrogen of P_{H2} = 35 MPa.

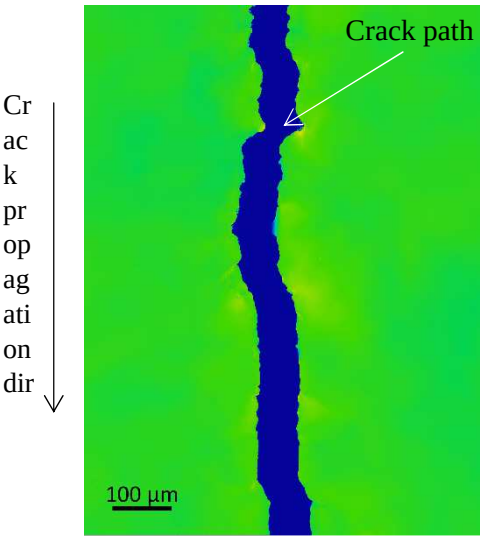

(d) At f = 20 Hz in hydrogen P_{H2} = 35 MPa.

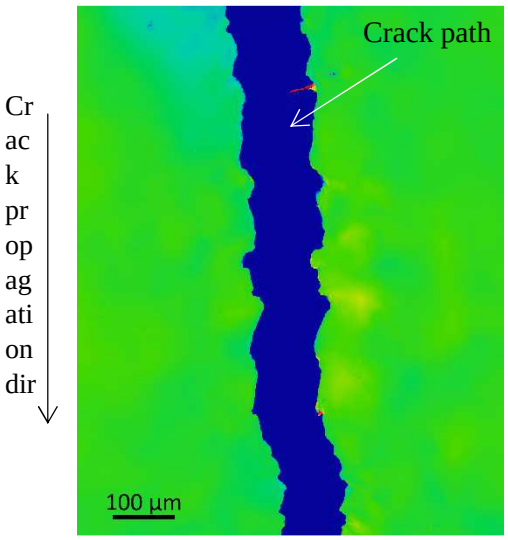

(e) At f = 2 Hz in hydrogen of P_{H2} = 3.5 MPa.

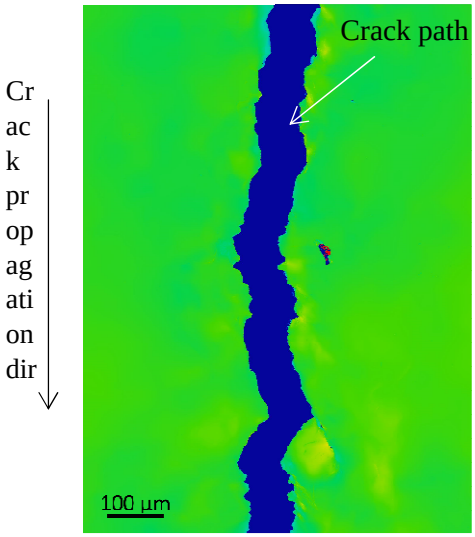

(f) At f = 20 Hz in hydrogen of P_{H2} = 3.5 MPa.

Fig. 8 Surface topography (height variation) of side surface near the crack path at ΔK = 18 MPa×m$^{1/2}$ in nitrogen and hydrogen at various hydrogen gas pressures and loading frequencies. The arrow shows the crack propagation direction from top to bottom in these images.

4. Discussion

The results presented in the previous section have clearly evidenced the influence of gaseous hydrogen on the FCGR and the crack tip plasticity in Armco iron. In addition, the dependencies of the HAFCG rate on the ΔK value, the hydrogen gas pressure $P_{H2,}$ and the loading frequency f have been identified. This section presents discussions on the fracture mechanisms prevailing in both the non-accelerated regime and the accelerated regime and the dependency of HAFCG on the parameters (ΔK, P_{H2}, and f).

4.1. Mechanism of hydrogen-induced intergranular fracture in the non-accelerated regime

Firstly, a mechanism of HAFCG in the non-accelerated regime is discussed in this section. Although no FCGR acceleration in hydrogen was observed at low ΔK values, a significant change in fracture mode occurred from a transgranular fracture in the air to an intergranular one in hydrogen. An interesting feature at micro-scale of this intergranular fracture is the formation of stripe-like markings on intergranular facets (Fig. 6b). These stripe-like markings have also been reported in some other researches [12,18,43–47]. Its nature can be an important clue for understanding the mechanism of the hydrogen-induced intergranular fracture. To investigate this point, the spacing of markings was measured at the different test conditions and at the different ΔK values by counting the number of markings crossing a perpendicular gauge line of length from 5 to 20 μm in the SEM images of fracture surface in each testing condition. An example of the gauge line (10 μm) is shown by the red line in Fig. 6c. The inclination of the intergranular facet plane was not considered in this measurement. 5 to 12 measurements were performed for a given test condition. The result is presented in Fig. 9. The plots and the error bars show the average value of the marking spacing and the standard deviation in each condition, respectively. The average values do not seem to depend on the test conditions (ΔK, the hydrogen gas pressure, and the loading frequency). The average value is approximately 0.65 μm which is one or two orders higher than the crack propagation distance per cycle (in

the order of 10^{-9} - 10^{-8} m), indicating that the spacing of markings is not corresponding to the macroscopic FCGR. Hence, the stripe-like marking is unlikely a striation.

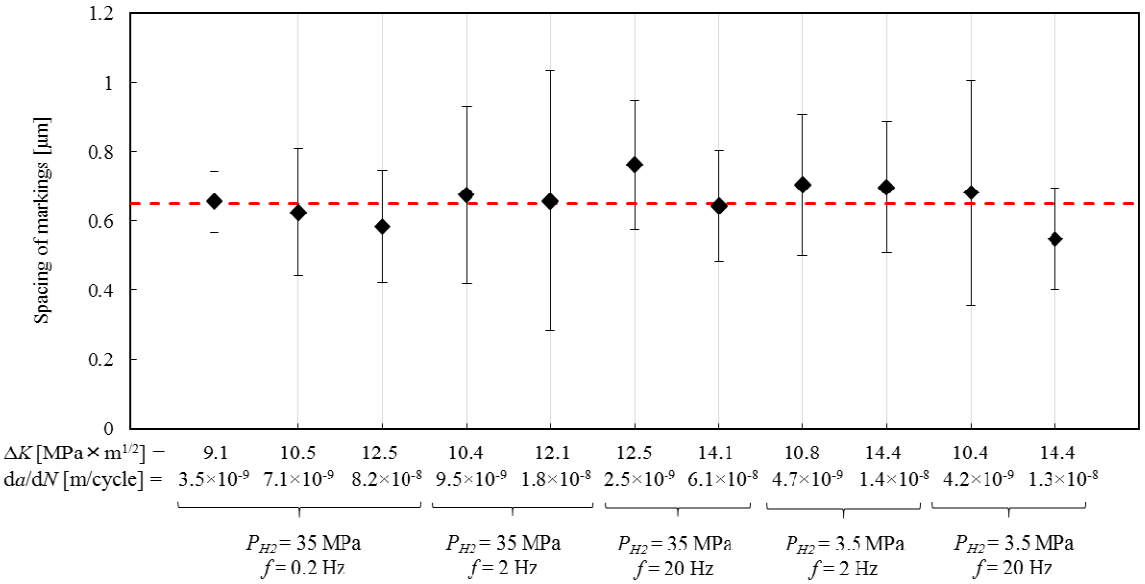

Fig. 9 Spacing of stripe-like markings observed on the surface of intergranular facets at various ΔK values, loading frequencies, and hydrogen gas pressures.

On the other hand, TEM observation of the cross-section beneath the intergranular facet in Armco iron by Shinko et al. [32] has revealed the presence of dislocation cell structure as shown in Fig. 10. The presence of dislocation cell structure is an evidence of a certain degree of plastic strain introduced into the grains ahead of the crack tip during the hydrogen-induced intergranular fracture. The accumulation of plastic strain ahead of the intergranular crack has also been confirmed by an in-situ observation of intergranular fatigue crack propagation in low carbon steel under gaseous hydrogen [43] and TEM observations of dislocation structure beneath intergranular facets in pure iron [45] and pure nickel [44,48].

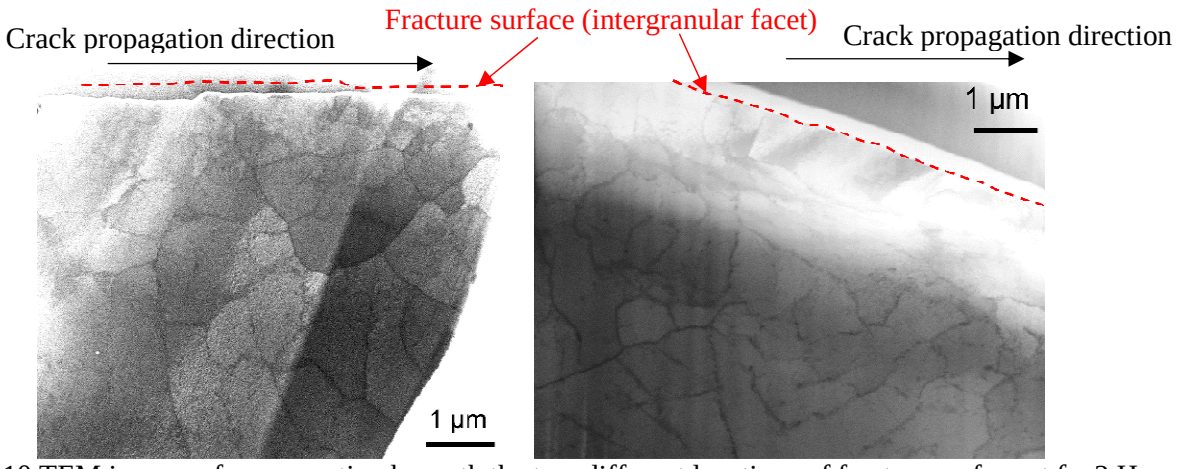

Fig. 10 TEM images of cross-section beneath the two different locations of fracture surface at f = 2 Hz

and ΔK = 11 MPa×m$^{1/2}$ in gaseous hydrogen of P_{H2} = 35 MPa [32]. The cell structure of dislocation is developed immediately beneath the fracture surface.

Based on this configuration of plastic strain related to the intergranular cracking, a mechanism of the hydrogen-induced intergranular fracture may be explained as follows. Hydrogen atoms diffused from the crack tip are dragged by mobile dislocations along slip planes. Since the grain boundary may act as a barrier for the dislocation mobility [49], the dislocations carrying hydrogen atoms stop and pile-up at the intersections of the slip plane and the grain boundary. The accumulated dislocations and hydrogen atoms may promote the nucleation of microvoids, as evidenced by Nagumo et al. [50,51]. The microvoids are linearly arranged at the intersection of slip plane and grain boundary and are possibly observed as stripe-like markings on the intergranular facets. Finally, the highly accumulated microvoids and hydrogen atoms at the grain boundaries weaken the bonding energy of the grain boundary, triggering a separation of grain boundary. Molecular dynamics simulations by Wang et al. [52] agree well with this grain boundary decohesion process.

A similar explanation of intergranular fracture has been recently proposed by Ogawa et al. [53]. They confirmed the presence of microvoids formed along the grain boundary during the intergranular cracking in a pure iron. Their model advocates that the dislocations and hydrogen atoms accumulated at grain boundaries cause a formation of microvoids and their coalescence results in intergranular crack propagation, in similar manner to the present model. In addition to this, they argued that hydrogen enhances the emission and mobility of dislocations inside of the grains ahead of the crack, playing an important role for a high amount of accumulation of dislocation and hydrogen at the grain boundary. Also, Wang et al. [45] have proposed a similar model for explaining an intergranular fracture in hydrogen-charged pure iron under monotonic loading. The “plasticity-mediated hydrogen-induced intergranular fracture process” seems to hold true for both cases of cyclic and monotonic loadings.

One more question remains: despite such a drastic change in the fracture mode from transgranular to intergranular due to the presence of hydrogen, the FCGR was not changed. One possible explanation for this is that the same level of strain energy might be required for triggering both types of cracking. The TEM observation of dislocation structure [32] has revealed that the size of dislocation cells formed beneath the fracture surface in air and hydrogen is almost the same, indicating that the same degree of plastic strain was imparted to the material during the crack propagation. This suggests that the same level of strain energy is consumed for plastic deformation during the transgranular crack propagation in air and the intergranular one in hydrogen. Thus, because the remaining available energy for crack advancement is the same for both cases, so the crack growth rate becomes almost the same. On the other hand, Ogawa et al. [53] explained this issue by a competition of two different effects of hydrogen, material softening (resulting in FCG deceleration) and material hardening (resulting in FCG acceleration), occurring at the same time.

4.2. Mechanism of hydrogen-induced QC fracture in the accelerated regime

According to the classification of environmentally assisted fatigue crack growth behavior [54], the HAFCG acceleration in Armco iron is considered as a stress-dependent process. ΔK_{tr} is similar to the threshold value of K for the onset of stress-corrosion cracking, K_{ISCC}, which does not depend on time (that is, a loading frequency). This is consistent with the present result: the value of ΔK_{tr} does not change with the loading frequency.

From the results of the surface topography measurement of the side surface near the crack tip presented in Section 3.3, it has been shown that hydrogen reduces the cyclic plastic deformation ahead of

the crack tip in the accelerated regime. The observed QC fracture surface with cleavage-like facets in this regime is another indicator of less plastic deformation cumulated at the crack tip prior to failure. This reduced plasticity is clearly associated with the FCGR enhancement due to hydrogen. In addition, the TEM observation of dislocation structure immediately beneath the fracture surface in the accelerated regime by Shinko et al. [32] has clarified that the dislocation structure in hydrogen is a random distribution of dislocation tangles without a development of cell structure, while a dislocation cell structure is formed in air. This result has revealed that hydrogen has a reduction effect of the crack tip plasticity. This plasticity reduction effect by hydrogen may be understood by referring to the hydrogen effects suppressing dislocation emission [55] and mobility [56,57]. The suppression of dislocation emission by hydrogen has been confirmed by molecular dynamics simulations by Song et al. [55] demonstrating that in hydrogen-rich regions, dislocation emission is blocked on the crack surface, and brittle cleavage occurs after increasing the applied loading. On the other hand, molecular dynamics simulations by Taketomi et al. [56,57] have confirmed that hydrogen induces the dislocation mobility reduction resulting in a hardening effect. These analytical results have been confirmed experimentally by the tensile test of hydrogen-charged pure iron by Kimura et al. [58–60] and microcantilever bending test in hydrogen charged-Fe-3%Si alloy by Hajilou et al. [61]. These hydrogen effects suppressing dislocation activity explain well the crack-tip plasticity reduction by hydrogen observed in this study (Fig. 8).

Based on these hydrogen effects, a scenario of the brittle QC fracture in the accelerated regime is proposed as follows. Solute hydrogen atoms diffused from the crack tip may accumulate in high hydrostatic stress regions ahead of the crack tip [62] during applied loading increases. The crack tip does not highly blunt because of the reduction of crack tip plasticity by hydrogen. The sharp crack tip causes high stress intensity and high hydrogen concentration in the vicinity of the crack tip. When both stress intensity and hydrogen concentration reach a critical level, cleavage fracture occurs by the HEDE mechanism [7] in which the hydrogen reduces bonding energy of matrix atoms. The cleavage fracture continues until the crack tip advances to the place containing insufficient amount of hydrogen concentration to continue the cleavage fracture.

An idea of hydrogen-induced cyclic cleavage fracture model was originally proposed by Marrow et al. [63]. Birenis et al. [40,41] have recently proposed a similar model to the present one in this study, involving a reduction of crack tip plasticity. Birenis's model states that the hydrogen-induced cleavage fracture is mainly contributed by a reduction of screw dislocation mobility rather than the bonding energy reduction of matrix atoms. On the other hand, as mentioned in Section 1, Matsuoka et al. [14,15] have proposed the HESFCG model based on the HELP mechanism. Nishikawa et al. [16] proposed the model based on a hydrogen-enhanced microvoid coalescence. However, both of these models assume that the hydrogen enhances local plasticity at the crack tip in the accelerated regime, which was not confirmed by the TEM observations by Shinko et al. [32] and Birenis et al. [40,41].

4.3. Influence of hydrogen gas pressure and loading frequency on HAFCG

From the results of the FCG tests at various hydrogen gas pressures and loading frequencies, the clear influence of testing condition has been confirmed. Specifically, in terms of the dependence of HAFCG rate on hydrogen gas pressure, the value of ΔK_{tr} decreases by increasing the hydrogen gas pressure. In terms of the dependence of HAFCG rate on loading frequency, the magnitude of FCGR enhancement in the accelerated regime increases by decreasing the loading frequency.

In order to investigate a cause and effect relationship between the testing conditions and a diffused hydrogen concentration C_H ahead of the crack tip, hydrogen diffusion from the crack tip during one

loading cycle has been calculated by the one-dimensional Fick's diffusion law in a semi-infinite plane surface subjected to a hydrogen concentration C_s, which can be approximated by an error function [64] as follows:

$$C_H(x,t) = C_s\left\{1 - erf\left(\frac{x}{2\sqrt{Dt}}\right)\right\} \tag{2}$$

where x is the distance from the surface of the semi-infinite plane, t the time, erf the error function, and D the diffusivity coefficient. The value of D is 2.5×10^{-10} m^2/s which was determined by a permeation test performed on the undeformed Armco iron [65]. To obtain C_H for one loading cycle period, the time t was given as $1/f$ [s]. The saturated hydrogen concentration at the surface C_s was obtained by Sievert's law [66]:

$$C_s = S_0\sqrt{P_{H2}}\exp\left(-\frac{\Delta H}{RT}\right) \tag{3}$$

where, S_0 is a constant, P_{H2} the hydrogen gas pressure, ΔH the dissolution enthalpy, R the gas constant, and T the absolute temperature. Fig. 11 shows the calculated hydrogen concentration ahead of the crack tip during one loading cycle. In this figure, hydrogen concentration is indicated as a ratio of C_H to the saturated hydrogen content at P_{H2} = 35 MPa, $C_{s,PH2=35}$. Although these calculations neglect some factors influencing hydrogen diffusion, such as the effects of crack tip plasticity and microstructure, they provide reliable orders of magnitude of hydrogen concentration.

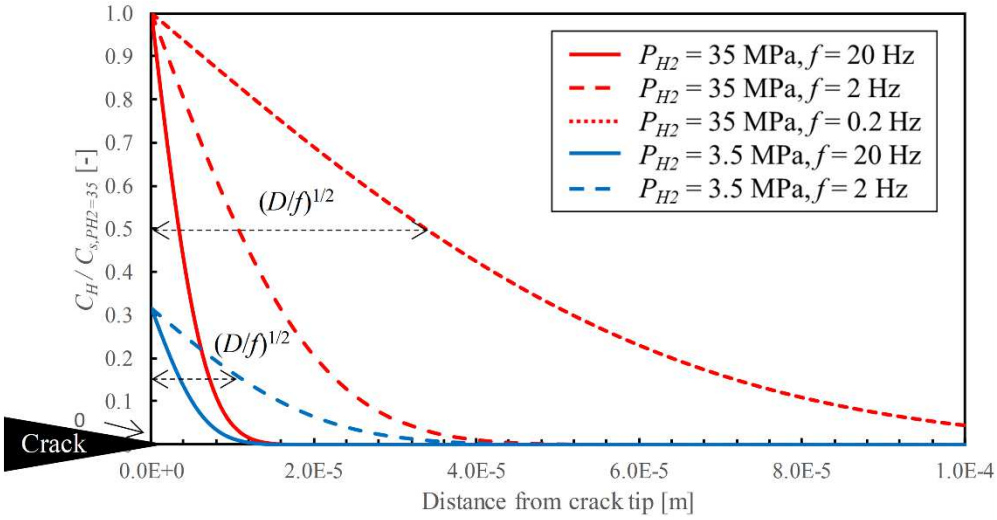

Fig. 11 Comparison of hydrogen concentration ahead of the crack tip during one loading cycle.

In terms of the influence of hydrogen gas pressure, Eq. (3) expresses that the saturated hydrogen content C_s depends on hydrogen gas pressure P_{H2} as shown in Fig. 11. Since ΔK_{tr} depends on hydrogen gas pressure as observed in Fig. 2, C_s is considered as an influential factor acting on the shift of ΔK_{tr}.

This dependence of ΔK_{tr} on hydrogen gas pressure agrees well the aforementioned mechanism assuming that certain levels of stress intensity and hydrogen concentration at the crack tip are required to trigger the hydrogen-induced QC fracture associated with the FCGR enhancement. If the hydrogen gas pressure is high, the hydrogen concentration at the crack tip (C_s) becomes also high, hence the hydrogen-induced QC fracture may be easily activated at an even low level of stress intensity at the crack tip. On the

contrary, if the hydrogen gas pressure is low, the hydrogen concentration at the crack tip (C_s) becomes low, hence a high level of stress intensity at the crack tip might be required to activate the hydrogen-induced QC fracture. This assumption explains the dependency of ΔK_{tr} on hydrogen gas pressure. A similar mechanism has also been suggested by Ogawa et al. [53].

In terms of the effect of loading frequency, the penetration depth $(D/f)^{1/2}$, which is defined as a distance from the crack tip where the value of C_H/C_s becomes 0.5 C_s, increases with the decrease in loading frequency (as shown in Fig. 11). This is because, at lower loading frequency, a longer period of one loading cycle allows hydrogen to diffuse deeper from the crack tip. According to the hydrogen-induced cyclic cleavage model (mentioned in Sub-section 4.2), deeper hydrogen penetration ahead of the crack tip may cause longer crack advancement due to the cleavage fracture, resulting in higher FCGR.

Another noticed fact about the loading frequency effect on the HAFCG rate is that the difference of the enhanced FCGR between f = 0.2 and 2 Hz is smaller compared to the one between f = 2 and 20 Hz. This suggests that there is likely a presence of an upper limit of the FCG enhancement by decreasing the loading frequency lower than 0.2 Hz. As mentioned in Section 1, the presence of an upper limit of the FCGR enhancement when the loading frequency decreases down to 10^{-3} Hz has been highlighted by several researches [14,24–27]. The value of this upper limit and its condition of loading frequency depend on hydrogen gas pressure [27] (or pre-charged hydrogen content [26]). If the upper limit also exists in the present case of Armco iron, the loading frequency dependency of FCGR in hydrogen (described in Fig. 4) is valid as long as the loading frequency is higher than the value at which the FCGR reaches to the upper limit. To verify this point, it is necessary to investigate the FCGR at lower loading frequency.

Furthermore, as also mentioned in Section 1, the research group at Kyushu University [26–28,67,68] has revealed that, at the loading frequency lower than the value at which HAFCG rate reaches the upper limit, a significant decrease in HAFCG rate occurs at relatively low hydrogen gas pressure (P_{H2} < 10 MPa) in several types of steels. The loading frequency causing this reduction of FCGR enhancement depends on the hydrogen gas pressure. Based on their experimental results, Yoshikawa et al. [27,28] have established a criterion for this phenomenon involving the parameter $(P_{H2} \times f)^{1/2}$. In their case of low carbon steel, the drop of FCGR enhancement occurs when $(P_{H2} \times f)^{1/2}$ is lower than 0.2 $(\mathrm{MPa/s})^{1/2}$. This parameter $(P_{H2} \times f)^{1/2}$ represents the gradient of hydrogen concentration ahead of the crack tip, more precisely the slope between C_s at the crack tip and C_H/C_s = 0.5 at the penetration depth $(D/f)^{1/2}$. In the case of this study in Armco iron, the FCGR enhancement was observed even at the lowest value of $(P_{H2} \times f)^{1/2}$ = 2.6 $(\mathrm{MPa/s})^{1/2}$ at the two conditions (P_{H2} = 35 MPa, f = 0.2 Hz and P_{H2} = 3.5 MPa, f = 2 Hz). On the other hand, Somerday et al. [24] suggested that the attenuation of the hydrogen effect may be controlled by the amount of oxygen in the hydrogen gas.

However, $(P_{H2} \times f)^{1/2}$ does not seem to be able to capture all the complexity of the FCGR enhancement drop because it does not take into account the value of ΔK at the onset of FCGR enhancement (ΔK_{tr}). For example, the two testing conditions P_{H2} = 35 MPa, f = 0.2 Hz and at P_{H2} = 3.5 MPa, f = 2 Hz are characterized by the same value of $(P_{H2} \times f)^{1/2}$ = 2 $(\mathrm{MPa/s})^{1/2}$, but the values of ΔK_{tr} are different as shown in Fig. 2. These values of ΔK_{tr} should be consistent if ΔK_{tr} was also controlled by $(P_{H2} \times f)^{1/2}$. Therefore, ΔK_{tr} cannot be determined only by $(P_{H2} \times f)^{1/2}$. This might be because the mechanism causing the onset of the FCGR enhancement according to ΔK_{tr} and $(P_{H2} \times f)^{1/2}$ are different: ΔK_{tr} is determined by the absolute hydrogen concentration at the crack tip (i.e. C_s) as mentioned above, while $(P_{H2} \times f)^{1/2}$ is determined by a gradient of hydrogen concentration ahead of the crack tip. Despite this, it is very important in practice to identify criteria controlling the onset of hydrogen-induced FCGR enhancement. It would greatly contribute to the improvement of safety design and fatigue life prediction of hydrogen-related equipment. Since these two criteria are only assumptions obtained experimentally so far, further experimental data

and theoretical considerations are necessary to clarify their physical meaning and rules. In this point of view, fatigue crack propagation tests under ΔK constant at lower loading frequency than 0.2 Hz under various hydrogen gas pressures are in progress. Also, it is planned to examine the modification of crack tip plasticity by hydrogen in more detail by means of TEM and EBSD observations.

5. Conclusions

The fatigue crack propagation in commercially pure iron, Armco iron, under gaseous hydrogen at P_{H2} = 3.5, 35 MPa at f = 0.2, 2, 20 Hz have been investigated aiming to clarify the dependency of HAFCG on the hydrogen gas pressure and the loading frequency and its mechanism. The influence of hydrogen on the fracture mode and the plastic deformation in the vicinity of the crack tip have been examined by means of the fracture surface observation and the surface topography measurement of the side surface near the crack path, in order to interpret the observed hydrogen effects on the fatigue crack growth resistance. The main conclusions are summarized below.

1) HAFCG rate exhibits three distinct regimes: a non-accelerated regime at low ΔK values, a transition regime, and an accelerated regime at high ΔK values showing FCGR enhancement up to 50 times higher than the FCGR in the air.
2) In the non-accelerated regime, the FCGR in hydrogen is almost the same compared to the one in the air. Fracture mode in hydrogen is a brittle intergranular fracture, in contrast to transgranular in the air at the same ΔK value. Furthermore, stripe-like plastic marking has been observed on intergranular facets. Based on these results and previously obtained ones from the TEM observation of dislocation structure, a scenario of hydrogen-induced intergranular fracture might be: mobile dislocations carrying hydrogen atoms accumulate at grain boundary ahead of the crack tip. Highly accumulated dislocations and hydrogen atoms induce microvoid nucleation which weakens the bonding energy of grain boundary, resulting in a grain boundary decohesion.
3) In the transition regime, fracture mode gradually changes from intergranular fracture to transgranular QC one, at the same time HAFCG rate highly increases. After the FCGR acceleration reaches a certain magnitude, the slope of HAFCG rate curve comes back to the same level as in the air, i.e. the accelerated regime. In the accelerated regime, fracture surface is fully covered by the QC fracture surface with brittle-like striations. The surface topography measurement of side surface near the crack path has revealed that hydrogen drastically reduces cyclic plastic deformation in the vicinity of the crack tip. A scenario of hydrogen-induced QC fracture has been proposed as follows: concentrated hydrogen atoms reduce the crack tip plasticity, inducing less blunting of the crack tip. Consequently, when the stress intensity and the hydrogen concentration at the crack tip reach a critical level, cleavage fracture occurs by HEDE mechanism.
4) Higher hydrogen gas pressure decreases the value of ΔK_{tr}. Besides, lower loading frequency increases the FCGR enhancement in the accelerated regime. These dependencies on the hydrogen gas pressure and the loading frequency may be explained in terms of C_s and $(D/f)^{1/2}$, respectively. Another important feature regarding the dependences is that there are likely two criteria of the onset of hydrogen effects defined by certain values of ΔK (i.e. ΔK_{tr}) and the hydrogen gradient (i.e. $(P_{H2} \times f)^{1/2}$). Identification of these criteria is practically important for improving safety design and fatigue life prediction of hydrogen-related equipment.

Acknowledgment:

Funding from the Poitou-Charentes region (G. Bilotta and T. Shinko Ph.D. thesis grants) is gratefully acknowledged. This work pertains to the French Government program “Investissements d’Avenir” (LABEX INTERACTIFS, reference ANR-11-LABX-0017-01).

References:

[1] Yoshida T, Kojima K. Toyota MIRAI Fuel Cell Vehicle and Progress Toward a Future Hydrogen Society. Interface Mag 2015;24:45–9. doi:10.1149/2.F03152if.

[2] Hénaff G, Odemar G, Tonneau-Morel A. Environmentally-assisted fatigue crack growth mechanisms in advanced materials for aerospace applications. Int J Fatigue 2007;29:1927–40. doi:10.1016/j.ijfatigue.2007.03.014.

[3] Murakami Y, Matsuoka S. Effect of hydrogen on fatigue crack growth of metals. Eng Fract Mech 2010;77:1926–40. doi:10.1016/j.engfracmech.2010.04.012.

[4] Lynch SP. Mechanisms and Kinetics of Environmentally Assisted Cracking: Current Status, Issues, and Suggestions for Further Work. Metall Mater Trans A 2012;44:1209–29. doi:10.1007/s11661-012-1359-2.

[5] Nanninga N, Slifka A, Levy Y, White C. A review of fatigue crack growth for pipeline steels exposed to hydrogen. J Res Natl Inst Stand Technol 2010;115:437. doi:10.6028/jres.115.030.

[6] Johnson WH. On Some Remarkable Changes Produced in Iron and Steel by the Action of Hydrogen and Acids. Proc R Soc London 1874;23:168–79. doi:10.1098/rspl.1874.0024.

[7] Oriani RA, Josephic PH. Testing of the decohesion theory of hydrogen-induced crack propagation. Scr Metall 1972;6:681–8. doi:10.1016/0036-9748(72)90126-3.

[8] Oriani RA. A Mechanistic Theory of Hydrogen Embrittlement of Steels. Berichte Der Bunsengesellschaft, Technol Asp 1972;76:848–57. doi:https://doi.org/10.1002/bbpc.19720760864.

[9] Birnbaum HK, Sofronis P. Hydrogen-enhanced localized plasticity-a mechanism for hydrogen-related fracture. Mater Sci Eng A 1994;176:191–202. doi:10.1016/0921-5093(94)90975-X.

[10] Lynch SP, Ryan NE. Mechanisms of Hydrogen Embrittlement - Crack Growth in a Low-Alloy Ultra-High-Strength Steel Under Cyclic and Sustained Stresses in Gaseous Hydrogen. Proc Second Int Congr Hydrog Met 1977:369–76.

[11] Takakuwa O, Yamabe J, Matsunaga H, Matsuoka S, Furuya Y. Comprehensive Understanding of Ductility Loss Mechanisms in Various Steels with External and Internal Hydrogen. Metall Mater Trans A Phys Metall Mater Sci 2017;48:5717–32. doi:10.1007/s11661-017-4323-3.

[12] Robertson IM, Sofronis P, Nagao A, Martin ML, Wang S, Gross DW, et al. Hydrogen Embrittlement Understood. Metall Mater Trans A Phys Metall Mater Sci 2015;46:2323–41. doi:10.1007/s11661-015-2836-1.

[13] Sun Z, Moriconi C, Benoit G, Halm D, Henaff G. Fatigue Crack Growth under High Pressure of Gaseous Hydrogen in a 15-5PH Martensitic Stainless Steel: Influence of Pressure and Loading Frequency. Metall Mater Trans A 2012;44:1320–30. doi:10.1007/s11661-012-1133-5.

[14] Matsuoka S, Tsutsumi N, Murakami Y. Effects of Hydrogen on Fatigue Crack Growth and Stretch Zone of 0.08mass%C Low Carbon Steel Pipe. Trans Japan Soc Mech Eng Ser A (in Japanese) 2008;74:1528–37. doi:10.1299/kikaia.74.1528.

[15] Murakami Y, Kanezaki T, Mine Y, Matsuoka S. Hydrogen Embrittlement Mechanism in Fatigue of Austenitic Stainless Steels. Metall Mater Trans A 2008;39:1327–39. doi:10.1007/s11661-008-9506-5.

[16] NISHIKAWA H, ODA Y, NOGUCHI H. Investigation of the Mechanism for Brittle-Striation Formation in Low Carbon Steel Fatigued in Hydrogen Gas. J Solid Mech Mater Eng 2011;5:370–85. doi:10.1299/jmmp.5.370.

[17] Nishikawa H, Oda Y, Takahashi Y, Noguchi H. Microscopic Observation of the Brittle-Striation Formation Mechanism in Low Carbon Steel Fatigued in Hydrogen Gas. J Solid Mech Mater Eng 2011;5:179–90. doi:10.1299/jmmp.5.179.

[18] Ogawa Y, Birenis D, Matsunaga H, Thøgersen A, Prytz Ø, Takakuwa O, et al. Multi-scale observation of hydrogen-induced, localized plastic deformation in fatigue-crack propagation in a pure iron. Scr Mater 2017;140:13–7. doi:10.1016/j.scriptamat.2017.06.037.

[19] Takahashi Y, Sakamoto J, Tanaka M, Higashida K, Noguchi H. Effect of hydrogen on dislocation structures around a mixed-mode fatigue crack tip in a single-crystalline iron-silicon alloy. Scr Mater 2011;64:721–4. doi:10.1016/j.scriptamat.2010.12.032.

[20] Takahashi Y, Tanaka M, Higashida K, Noguchi H. Hydrogen-induced slip localization around a quasi-brittle fatigue crack observed by high-voltage electron microscopy. Scr Mater 2009;61:145–8. doi:10.1016/j.scriptamat.2009.03.020.

[21] Martin ML, Sofronis P, Robertson IM, Awane T, Murakami Y. A microstructural based understanding of hydrogen-enhanced fatigue of stainless steels. Int J Fatigue 2013;57:28–36. doi:10.1016/j.ijfatigue.2012.08.009.

[22] Martin ML, Robertson IM, Sofronis P. Interpreting hydrogen-induced fracture surfaces in terms of deformation processes: A new approach. Acta Mater 2011;59:3680–7. doi:10.1016/j.actamat.2011.03.002.

[23] Bilotta G, Arzaghi M, Hénaff G, Benoit G, Halm D. Hydrogen Induced Intergranular Failure in Armco Iron Under Fatigue Crack Propagation. Vol 6B Mater Fabr 2016:V06BT06A026. doi:10.1115/PVP2016-63338.

[24] Somerday BP, Sofronis P, Nibur KA, Marchi CS, Kirchheim R. Elucidating the variables affecting accelerated fatigue crack growth of steels in hydrogen gas with low oxygen concentrations. Acta Mater 2013;61:6153–70. doi:10.1016/j.actamat.2013.07.001.

[25] Matsuoka S, Tanaka H, Homma N, Murakami Y. Influence of hydrogen and frequency on fatigue crack growth behavior of Cr-Mo steel. Int J Fract 2011;168:101–12. doi:10.1007/s10704-010-9560-z.

[26] Macadre A, Artamonov M, Matsuoka S, Furtado J. Effects of hydrogen pressure and test frequency on fatigue crack growth properties of Ni-Cr-Mo steel candidate for a storage cylinder of a 70MPa hydrogen filling station. Eng Fract Mech 2011;78:3196–211. doi:10.1016/j.engfracmech.2011.09.007.

[27] Yamabe J, Yoshikawa M, Matsunaga H, Matsuoka S. Effects of hydrogen pressure, test frequency and test temperature on fatigue crack growth properties of low-carbon steel in gaseous hydrogen. Procedia Struct Integr 2016;2:525–32. doi:10.1016/j.prostr.2016.06.068.

[28] Yoshikawa M, Matsuo T, Tsutsumi N, Matsunaga H, Matsuoka S. Effects of hydrogen gas pressure and test frequency on fatigue crack growth properties of low carbon steel in 0.1-90 MPa

hydrogen gas. Trans JSME (in Japanese) 2014;80:SMM0254-SMM0254. doi:10.1299/transjsme.2014smm0254.

[29] Moriconi C, Hénaff G, Halm D. Cohesive zone modeling of fatigue crack propagation assisted by gaseous hydrogen in metals. Int J Fatigue 2014;68:56–66. doi:10.1016/j.ijfatigue.2014.06.007.

[30] Bilotta G, Hénaff G, Benoit G, Moriconi C, Halm D, Arzaghi M. Cohesive Zone Modeling Of Hydrogen Assisted Cracking In A 15-5 PH Steel And Comparison With Experiments. ASME 2015 Press Vessel Pip Conf 2015:1–8. doi:10.1115/PVP201545631.

[31] Bilotta G, Arzaghi M, Benoit G, Halm D, Henaff G, Shinko T. Environmentally-Assisted Fatigue Crack Growth in ARMCO Iron Under High Pressure of Gaseous Hydrogen. Proc Int Hydrog Conf (IHC 2016) Mater Perform Hydrog Environ 2016:1–10. doi:10.1115/1.861387_ch21.

[32] Shinko T, Hénaff G, Halm D, Benoit G. Influence of gaseous hydrogen on plastic strain in vicinity of fatigue crack tip in Armco pure iron. MATEC Web Conf 2018;165:03006. doi:10.1051/matecconf/201816503006.

[33] Drexler ES, Slifka AJ, Amaro RL, Barbosa N, Lauria DS, Hayden LE, et al. Fatigue crack growth rates of API X70 pipeline steel in a pressurized hydrogen gas environment. Fatigue Fract Eng Mater Struct 2014;37:517–25. doi:10.1111/ffe.12133.

[34] Slifka AJ, Drexler ES, Stalheim DG, Amaro RL, Lauria DS, Stevenson AE, et al. The Effect of Microstructure on the Hydrogen-Assisted Fatigue of Pipeline Steels. Vol 6B Mater Fabr 2013:V06BT06A009. doi:10.1115/PVP2013-97217.

[35] Ronevich JA, Somerday BP, San Marchi CW. Effects of microstructure banding on hydrogen assisted fatigue crack growth in X65 pipeline steels. Int J Fatigue 2015;82:497–504. doi:10.1016/j.ijfatigue.2015.09.004.

[36] Ronevich JA, Somerday BP. Hydrogen Effects on Fatigue Crack Growth Rates in Pipeline Steel Welds. Vol 6B Mater Fabr 2016:V06BT06A035. doi:10.1115/PVP2016-63669.

[37] Bilotta G, Henaff G, Halm D, Arzaghi M. Experimental measurement of out-of-plane displacement in crack propagation under gaseous hydrogen. Int J Hydrogen Energy 2017;42:10568–78. doi:10.1016/j.ijhydene.2017.02.084.

[38] Yamabe J, Yoshikawa M, Matsunaga H, Matsuoka S. Hydrogen trapping and fatigue crack growth property of low-carbon steel in hydrogen-gas environment. Int J Fatigue 2017. doi:10.1016/j.ijfatigue.2017.04.010.

[39] Ogawa Y, Birenis D, Matsunaga H, Takakuwa O, Yamabe J, Prytz Ø, et al. Hydrogen-assisted fatigue crack propagation in a pure BCC iron. Part I: Intergranular crack propagation at relatively low stress intensities. MATEC Web Conf 2018;165:03011. doi:10.1051/matecconf/201816503011.

[40] Birenis D, Ogawa Y, Matsunaga H, Takakuwa O, Yamabe J, Prytz Ø, et al. Hydrogen-assisted fatigue crack propagation in a pure BCC iron. Part II: Accelerated regime manifested by quasi-cleavage fracture at relatively high stress intensity range values. MATEC Web Conf 2018;165:03010. doi:10.1051/matecconf/201816503010.

[41] Birenis D, Ogawa Y, Matsunaga H, Takakuwa O, Yamabe J, Prytz Ø, et al. Interpretation of hydrogen-assisted fatigue crack propagation in BCC iron based on dislocation structure evolution around the crack wake. Acta Mater 2018;156:245–53. doi:10.1016/j.actamat.2018.06.041.

[42] Rice JR. Mechanics of Crack Tip Deformation and Extension by Fatigue. Fatigue Crack Propag 1967;ASTM STP 4:247–309. doi:10.1520/STP47234S.

[43] Nishikawa H, Oda Y, Noguchi H. Investigation of Mechanism for Intergranular Fatigue Crack Propagation of Low Carbon Steel JIS S10C in Hydrogen Gas Environment. J Solid Mech Mater Eng 2011;5:263–78. doi:10.1299/jmmp.5.263.

[44] Martin ML, Somerday BP, Ritchie RO, Sofronis P, Robertson IM. Hydrogen-induced intergranular failure in nickel revisited. Acta Mater 2012;60:2739–45. doi:10.1016/j.actamat.2012.01.040.

[45] Wang S, Martin ML, Sofronis P, Ohnuki S, Hashimoto N, Robertson IM. Hydrogen-induced intergranular failure of iron. Acta Mater 2014;69:275–82. doi:10.1016/j.actamat.2014.01.060.

[46] Pokluda J, Siegl J. MIXED FATIGUE FRACTURE MORPHOLOGY OF FERRITIC DUCTILE IRON. Fatigue Fract Eng Mater Struct 1990;13:375–85. doi:10.1111/j.1460-2695.1990.tb00608.x.

[47] Koyama M, Onishi Y, Noguchi H. Characteristics of hydrogen-assisted intergranular fatigue crack growth in interstitial-free steel: role of plastic strain localization. Int J Fract 2017;206:123–30. doi:10.1007/s10704-017-0205-3.

[48] Lassila DH, Birnbaum HK. Intergranular fracture of nickel: the effect of hydrogen-sulfur co-segregation. Acta Metall 1987;35:1815–22. doi:10.1016/0001-6160(87)90127-1.

[49] Kacher J, Robertson IM. Quasi-four-dimensional analysis of dislocation interactions with grain boundaries in 304 stainless steel. Acta Mater 2012;60:6657–72. doi:10.1016/j.actamat.2012.08.036.

[50] Nagumo M. Function of hydrogen in embrittlement of high-strength steels. ISIJ Int 2001;41:590–8. doi:10.2355/isijinternational.41.590.

[51] Takai K, Shoda H, Suzuki H, Nagumo M. Lattice defects dominating hydrogen-related failure of metals. Acta Mater 2008;56:5158–67. doi:10.1016/j.actamat.2008.06.031.

[52] Wang S, Martin ML, Robertson IM, Sofronis P. Effect of hydrogen environment on the separation of Fe grain boundaries. Acta Mater 2016;107:279–88. doi:10.1016/j.actamat.2016.01.067.

[53] Ogawa Y, Birenis D, Matsunaga H, Takakuwa O, Yamabe J, Prytz Ø, et al. The role of intergranular fracture on hydrogen-assisted fatigue crack propagation in pure iron at a low stress intensity range. Mater Sci Eng A 2018. doi:10.1016/j.msea.2018.07.014.

[54] Vasudevan AK, Sadananda K. Classification of environmentally assisted fatigue crack growth behavior. Int J Fatigue 2009;31:1696–708. doi:10.1016/j.ijfatigue.2009.03.019.

[55] Song J, Curtin W a. Atomic mechanism and prediction of hydrogen embrittlement in iron. Nat Mater 2013;12:145–51. doi:10.1038/nmat3479.

[56] Taketomi S, Matsumoto R, Miyazaki N. Atomistic study of the competitive relationship between edge dislocation motion and hydrogen diffusion in alpha iron. J Mater Res 2011;26:1269–78. doi:10.1557/jmr.2011.106.

[57] Taketomi, S., Imanishi, S., Matsumoto, R., Miyazaki N. Dislocation dynamics analysis of hydrogen embrittlement in alpha iron based on atomistic investigations. 13th Int Conf Fract 2013:16–21.

[58] Matsui H, Kimura H, Moriya S. The effect of hydrogen on the mechanical properties of high purity iron I. Softening and hardening of high purity iron by hydrogen charging during tensile deformation. Mater Sci Eng 1979;40:207–16. doi:10.1016/0025-5416(79)90191-5.

[59] Moriya S, Matsui H, Kimura H. The effect of hydrogen on the mechanical properties of high purity iron II. Effect of quenched-in hydrogen below room temperature. Mater Sci Eng 1979;40:217–25. doi:10.1016/0025-5416(79)90192-7.

[60] Matsui H, Kimura H, Kimura A. The effect of hydrogen on the mechanical properties of high purity iron III. The dependence of softening in specimen size and charging current density. Mater Sci Eng 1979;40:227–34. doi:10.1016/0025-5416(79)90193-9.

[61] Hajilou T, Deng Y, Rogne BR, Kheradmand N, Barnoush A. In situ electrochemical microcantilever bending test: A new insight into hydrogen enhanced cracking. Scr Mater 2017;132:17–21. doi:10.1016/j.scriptamat.2017.01.019.

[62] Oriani RA, Josephic PH. Equilibrium aspects of hydrogen-induced cracking of steels. Acta Metall 1974;22:1065–74. doi:10.1016/0001-6160(74)90061-3.

[63] Marrow TJ, Cotterill PJ, King JE. Temperature effects on the mechanism of time independent hydrogen assisted fatigue crack propagation in steels. Acta Metall Mater 1992;40:2059–68. doi:10.1016/0956-7151(92)90192-H.

[64] Crank J. The mathematics of diffusion. Second edi. 1975.

[65] Bilotta G. Influence de l'hydrogène gazeux sur la vitesse de propagation d'une fissure de fatigue dans les métaux : approche expérimentale et modélisation. École nationale supérieure de mécanique et d'aérotechnique, 2016.

[66] Fukai Y. The Metal-Hydrogen System. vol. 21. Second edi. Springer; 2005. doi:10.1007/3-540-28883-X.

[67] Matsunaga H, Nakashima T, Yamada K, Matsuo T, Yamabe J, Matsuoka S. Effect of Test Frequency on Hydrogen-Enhanced Fatigue Crack Growth in Type 304 Stainless Steel and Ductile Cast Iron. Vol 6B Mater Fabr 2016:V06BT06A031. doi:10.1115/PVP2016-63536.

[68] Matsunaga H, Takakuwa O, Yamabe J, Matsuoka S. Hydrogen-enhanced fatigue crack growth in steels and its frequency dependence. Philos Trans R Soc A Math Phys Eng Sci 2017;375:20160412. doi:10.1098/rsta.2016.0412.